

MAPPING CLAY AND OXIDE-BASED ROCK MINERALS IN TROPICAL RAINFOREST USING LANDSAT-8 OLI

Mohammed Oludare Idrees^{1,4*}, Kouame Yao^{2,4}, Mohamed Barakat Gibril^{3,4}
Okoli Jude Emeka⁴ and Ipadeola Ademuyiwa Oyedapo¹

¹Department of Surveying and Geoinformatics, Faculty of Environmental Science, University of Ilorin, P.M.B. 1515, Ilorin, Nigeria.

²Department of Earth and Planetary Sciences, Faculty of Science and Engineering, Macquarie University, North Ryde, NSW 2109 Australia.

³GIS & Remote Sensing Center, Research Institute of Science and Engineering, University of Sharjah, 27272 Sharjah, UAE

⁴Department of Civil Engineering, Faculty of Engineering, Universiti Putra Malaysia 43400 UPM, Serdang, Selangor, Malaysia

Email: *mohammed.oi@unilorin.edu.ng, dare.idrees@gmail.com (corresponding author),
kouame_yao@aol.com, brakuta@hotmail.com, mario16@geologist.com, dapsen2010@gmail.com

ABSTRACT

Advances in Landsat satellite sensor development open opportunities for geological exploration, especially in vegetated environments. This study investigates the potentials of Landsat-8 OLI imagery for mapping clay and oxide-based rock minerals and visualization of lithological features under vegetation in tropical rainforest. The satellite image was spectrally transformed using Directed Principal Component Analysis (DPCA) which employs band ratio indices to derive the abundance of four major components: clay, ferric iron oxide, ferrous iron oxide, and vegetation spectral. DPCA transformation suppresses vegetation spectral in order to reveal both the physical and geochemical properties of the underlining rock surface. The result was further subjected to dimensionality reduction with Principal Component Analysis (PCA). Through analysis of the statistical Eigenvector, the three most informative directed principal component images were selected for lithological and geochemical analysis of the rocks. The greyscale image of DPC 2 best describes the physical properties of the lithology while RGB false colour composites of DPC 1, DPC 2, and DPC 3 highlights spatial variation (using the colour appearance) and the abundance of clay minerals, silica and iron oxide within the respective rock units. The result shows that both lithological and geochemical information of rocks under vegetation can be derived from Landsat-8.

Keywords: Remote sensing; Landsat-8; spectral transformation; geology; clay mineral; lithology

1. Introduction

Until latter half of the 20th century when the space opened to human exploration, Geologists have always relied only on site investigation and analysis of the physical and chemical properties of rock samples taking during such expedition. Today, remote sensing technology has revolutionized this arduous and time consuming practice. Spectral analysis of rock minerals from images acquired by air/space-borne sensors has taken geologic investigations and information gathering to an unprecedented level of precision especially when the bedrock is exposed to direct observation from space. However, in



tropical region, the surface is mostly covered by vegetation that inhibits rock spectral beneath vegetation canopy (Siegal and Goetz 1977, Murphy and Wadge 1994, Crippen and Blom 2001). NDVI (Normal Difference Vegetation Index) and vegetation masking have been widely used to differentiate vegetation from the soil spectral. NDVI requires that both spectra of vegetation and land surface be apparent on the image for the vegetation spectra to be suppressed through masking. Vegetation masking, on the other hand, enables better interpretation of geologic features through the removal of vegetation effect from the red and near infrared bands (Bahiru, 2011). The two approaches described are not widely used for geological investigation.

The last three decades have witnessed concerted efforts by many researchers to address interference of vegetation spectra. Early researchers explored vegetation reflectance suppression using spectral unmixing which determines the proportion of each material within an ensemble of a mixture (e.g. Horwitz *et al.* (1971), Smith *et al.* (1990), Mustard (1993), van der Meer (1995), van der Meer and de Jong (2000), Neville *et al.* (2003), Plaza *et al.* (2004), Crippen and Blom (2001)). Theoretically, spectral unmixing is simple and robust but approach cannot effectively yield outcome that is free of vegetation reflectance (Yu *et al.*, 2011). Moreover, the technique is sensitive to spectral resolution which makes it much more appropriate with hyperspectral data (van der Meer and de Jong 2000). Forced Invariance is another approach that attempts to solve vegetation spectral effect (Crippen and Blom 2001). Studies conducted in semi-arid regions with open canopy cover reveal the method is highly sensitive to vegetation volume; however, in terms of the lithology, it was observed to be insensitive in a linear ratio-versus-ratio plot (Elvidge and Lyon (1985a) and Fraser and Green (1987). So, Fraser and Green (1987) suggested further implementation of the method based on image comparison.

In line with Fraser's proposition, new ratios and band statistics algorithms were proposed by Rowan *et al.* (1992) and Crippen and Bloom (2001) respectively to enhance the performance of transformation technique. These efforts resulted to the two prominent transformation techniques, principal components analysis (PCA) and Directed Principal Component Analysis (DPCA), specifically for suppressing vegetation reflectance in optical data for geological investigation. PCA is a statistical multivariate method that reduces the data into series of interpretable views which stress on a natural grouping in the data (Marsili, 2006) such that variables that exhibits pronounced influence of patterns are highlighted (Singh and Harrison, 1985; Gad and Kusky, 2007; Qari *et al.*, 2008). DPCA permits to distinguish clay in the imagery by deriving ratios based on Landsat bands (Fraser and Green, 1987). Four mineral indices: vegetation, clay minerals, ferric iron oxide and ferrous iron oxide respectively represent the ratio of specific bands that are subjected to dimensionality reduction through PCA. Expectedly, each band ratio contains information of an enhanced lithology. The strength of these transformation techniques has been demonstrated in the extensive works of Pour and his co-researchers (Pour *et al.*, 2013; Pour and Hashim 2013 and 2014). This study employs spectral transformation to map clay and oxide-based rock minerals and to visualize the lithological features of the rock under vegetation using Landsat-8 OLI.

2. Geology of the study area

This study was conducted around Gua Musang area with long history of gold mineralization. Gua Musang is the largest district in Kelantan, a state in Peninsular Malaysia. Specifically, the study area lies between longitudes $101^{\circ}39' 50.86''\text{E}$ and $102^{\circ}7'13.04''\text{E}$, and latitudes $4^{\circ}40'45.65''\text{N}$ and $5^{\circ}6'31.92''\text{N}$ (Figure 1). In terms of climate, it is a typical tropical climate and average annual temperature of about 28°C . The site is characterized by a mix of thick and sparsely vegetation cover. Major economic activities in Gua Musang include agriculture, timber logging and gold mining. Strategically, the site is selected to cover the southern gold and silver mercury belt which spans the central part of the state in a North-South trending; measuring about 45124 square kilometres. The area is characterized with precious minerals and rocks comprising of a good spread within hydrothermal Quartz-veins (Heng *et al.* 2006).

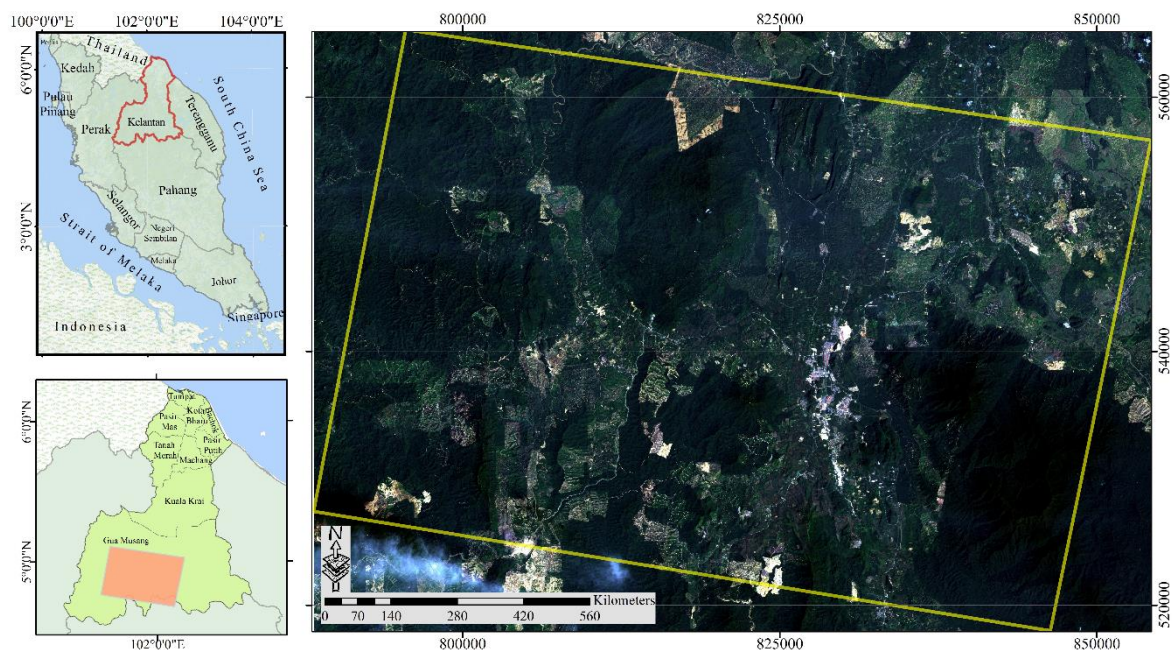


Fig.1: Location of the study area - Map of Peninsula Malaysia highlighting the State of Kelantan (top left), Gua Musang district (bottom left) true colour composite of Landsat-8 (Right).

Previous studies reveals that the geology of Kelantan evolved through series of volcanic activities which has occasioned the present geological variability within the west, central, and eastern belts (Shah, 2012). The surficial lithology of the state of Kelantan comprises of igneous, sedimentary and metamorphic rocks, occurring in a north-south trending that conditioned the profile of mineralization zones to the west and eastern border lies igneous rock that forms the main range granite and boundary range granite respectively (Rahman and Mohamed, 2001). The main range granites belong to the middle Triassic age that comprises of intermediate intrusive igneous rock. The central belt of the state is composed of sedimentary and meta-sedimentary rocks of both Triassic and Permian age. The



Triassic sediment is a conglomerate of interbedded sandstone, siltstone and shale while the Permian counterpart contains phyllite, slate and shale with subordinate sandstone and schist. Also, the central belt is intersected by intermediate to basic volcanics, mainly pyroclastic sediment (Nazarudin, *et al.*, 2014). Details of the geology of Kelantan can be found in (Howard, 1967; Tjia, 1973; Rahman and Mohamed, 2001; Unjah *et al.*, 2001; Department of Minerals and Geoscience Malaysia, 2003; Ghani. 2009).

3. Material and methods

The Landsat-8 OLI image used in this study was acquired on February 4th, 2014. The data with 9% cloud coverage was provided free of charge by the United States Geological Survey (USGS) through its data depository (<http://earthexplorer.usgs.gov> and <http://glovis.usgs.gov>) online resources. Table 1 presents the properties of the Landsat data used.

Table 1: Properties of the Landsat data used

Bands	Spectrum	Wavelength	Resolution
Band 1	Deep blue and Violet	0.433 – 0.453	30 Meters
Band 2		0.450 – 0.515	
Band 3	Visible (Blue-Green-Red)	0.525 – 0.600	
Band 4		0.630 – 0.680	
Band 5	Near Infrared (TIR)	0.851 – 0.879	
Band 6	Shortwave Infrared (SWIR)	1.566 – 1.651	
Band 7		2.107 – 2.294	
Band 8	Panchromatic	0.503 – 0.676	15 m
Band 9	Cirrus Clouds	1.360 – 1.390	30m
Band 10	Thermal Infrared (TIR)	10.60 - 11.20	
Band 11		11.50 - 12.50	100m

3.1 Data pre-processing

The image was processed in ENVI4.8. The processing tasks commenced with pre-processing operations, generating image index and finally image transformation. Figure 2 is the step-by-step data processing and analysis workflow. The image came geometrically corrected; however, it was corrected for atmospheric effects using quick atmospheric correction (QUAC) technique (Markham *et. al.*, 2014). QUAC is simple to use because it determines atmospheric correction parameters from the spectra of the image scene without the need for any other external information (Guide, E.U.S., 2009). In addition, it is capable of producing accurate pixels that reasonably represent the image object spectra. Only the first seven bands (Coastal, visible bands, NIR and the two SWIR) were utilized for this study.

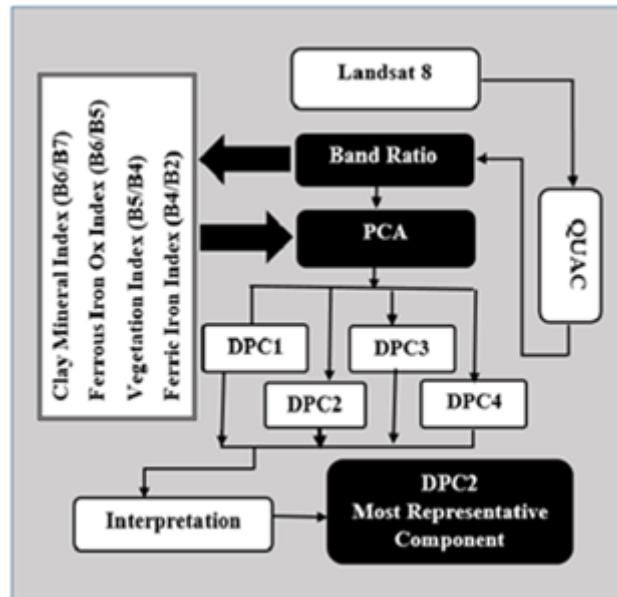


Fig. 2: Data processing and analysis workflow.

3.2 Spectral transformation

The DPCA proposed by Fraser and Green (1987) is a two-step processing chain that integrates two spectral transformation techniques, band ratio and principal component analysis (PCA). First, band ratios are generated from the image spectral bands and the results are subsequently subjected to PCA. This is an effective enhancement technique that is useful in discriminating different regolith materials (Wilford and Creasey, 2002). Band Ratio manipulates the spectral values of input bands to improve features identification by emphasizing certain characteristics or materials that cannot be visible in the individual bands (Inzana *et al.*, 2003). In this work, four band ratios representing different mineral indices were generated using the Landsat 8 image. They are: vegetation (Band 5/Band 4), Clay Mineral (Band 6/Band 7), Ferrous Iron (Band 6/Band 5), and Ferric Iron (Band 4/Band 2) (Ali and Pour, 2014). The ratio bands were further subjected to PCA transformation. The method has gained wide application for lithological mapping and mineral exploration (Sultan *et al.*, 1986; Swayze and Clark, 1995; Rowan *et al.*, 2003, 2005; Galvão *et al.*, 2005; Amer *et al.*, 2010; Aboelkhair *et al.*, 2010; Ramadan and Abdel Fattah, 2010).

PCA is a statistical multivariate method which employs uncorrelated linear combination technique of variables and transforms them into new data set with new correlated variables that reduce the discrepancy contained in the data (Singh and Harrison, 1985; Gad and Kusky, 2007; Qari *et al.*, 2008). PCA correlates inherent similarities in bands caused by redundant information to increase data dimensionality. This makes it a suitable technique for this study where the site is characterized by hydrothermally altered mineralization zone (Amer *et al.*, 2010; Pour and Hashim, 2011a, b, c, 2012a, b, 2013; Pour *et al.*, 2013a, 2014; Pournamdari and Hashim, 2013).

4. Results and Discussion

Analysis of the resulting DPCA Eigenvectors and values (Table 2) provides indicators of relevant components that best represents the target information.

Table 2: Eigenvectors and values of the DPCA images

Index	Vegetation Index	Ferrous Iron Oxide	Clay Mineral Index	Ferric Iron Oxide	Eigenvalues
Ratio	B5/B4	B6/B5	B6/B7	B4/B2	%
DPC 1	-0.067117	-0.996725	0.045077	0.001594	99.56%
DPC 2	-0.738147	0.079281	0.647945	0.170355	0.31%
DPC 3	0.15745	0.012551	-0.077902	0.98437	0.08%
DPC 4	0.652567	-0.009808	0.756351	-0.044646	0.05%

Decision about the information content of DPC images is usually based on statistical interpretation of the signs (positive and negative) in the resulting Eigenvector and values (Table 2). These signs are significant to the representative rock mineral constituent in the derived images. Negative (-) sign represent dark pixels that indicates low presence of a particular mineral element while the positive (+) sign display bright pixels that denote abundant presence of the target mineral content. Furthermore, the amount of rock mineral content abundance is also interpreted using the location of the value on the x-axis. For example, even though -0.067117 and -0.738147 values have negative signs, the former has more information content than the latter because it is closer to the positive zero on the axis. Evaluating the impact of vegetation suppression in the component images requires consideration with other mineral indices for better accuracy. Therefore, both quantitative and qualitative evaluation of the Eigenvector, values and the representative component images provide understanding of the results.

The first general quantitative indicator is the percentage of the Eigenvalues. DPC1, for instance, contains 99.56% of the features spectral information while DPC2, DPC3 and DPC4 have 0.31%, 0.08% and 0.05% respectively; meaning that the first two images are more informative than the last ones. Assessment of the Eigenvectors and signs of the individual mineral index reveals that DPC1 and DPC2 have negative vegetation content (-0.067117 and -0.738147) compare to DPC3 and DPC4 which has high presence of vegetation spectra (0.157450 and 0.652567). On the other hand, contributions of the three mineral indices (Clay, Ferric and Ferrous Iron Oxide) to the components do not follow directly the pattern in which vegetation appears. It can be observed that DPC2 contributes positively to the other mineral indices but minimally for Ferrous Iron Oxide. For DPC3 and DPC4, positive contribution of the vegetation index inhibits the amount of information about the surficial rock mineral underneath. DPC4 exhibits the highest statistically dominant image characterized by high scale unsuppressed vegetation. This is reflected in the strong presence of vegetation index that conflicts with strong presence of Al (OH) bearing clay mineral (0.756351). In addition to that, there is negative contribution of the two alteration mineral indices, Ferric and Ferrous iron oxide (-0.044646 and -0.009808). All these constitute divergent disturbances that constitute noise in DPC4 that renders it unsuitable for consideration Crippen and Blom (2001) and

Ryerson and Rencz (1999). Hence, DPCs 1, 2 and 3 were chosen for further analysis to map the target features.

4.1 Interpretation of the DPC images

Visual analysis of the DPC greyscale images reveal information about the rock surface beneath vegetation and further provides insight into the implications of the quantitative Eigenvector and values. In the figures, bright tone represents high variation while dark tone reveals low variation. The foregoing quantitative analysis leads to the conclusion that DPC1 image (Fig 3) contains most of the scene spectral information (Jensen, 2005); however, it is less sensitive to lithological variation because of low contribution of the clay (a hydroxyl-bearing in altered rocks) and ferrous iron oxide mineral spectral (0.045077 and -0.996725) respectively. Also, the input of ferric iron oxide (0.001594) is not sufficient to reveal the characteristic slope and relief of the lithology. This implies that DPC1 has significant presence of vegetation spectra; yet, sensitive to altered rocks (in bright tones) as a result of the prevailing presence of hydroxyl-bearing mineral in the image while the other information remain hiding (in dark tones).

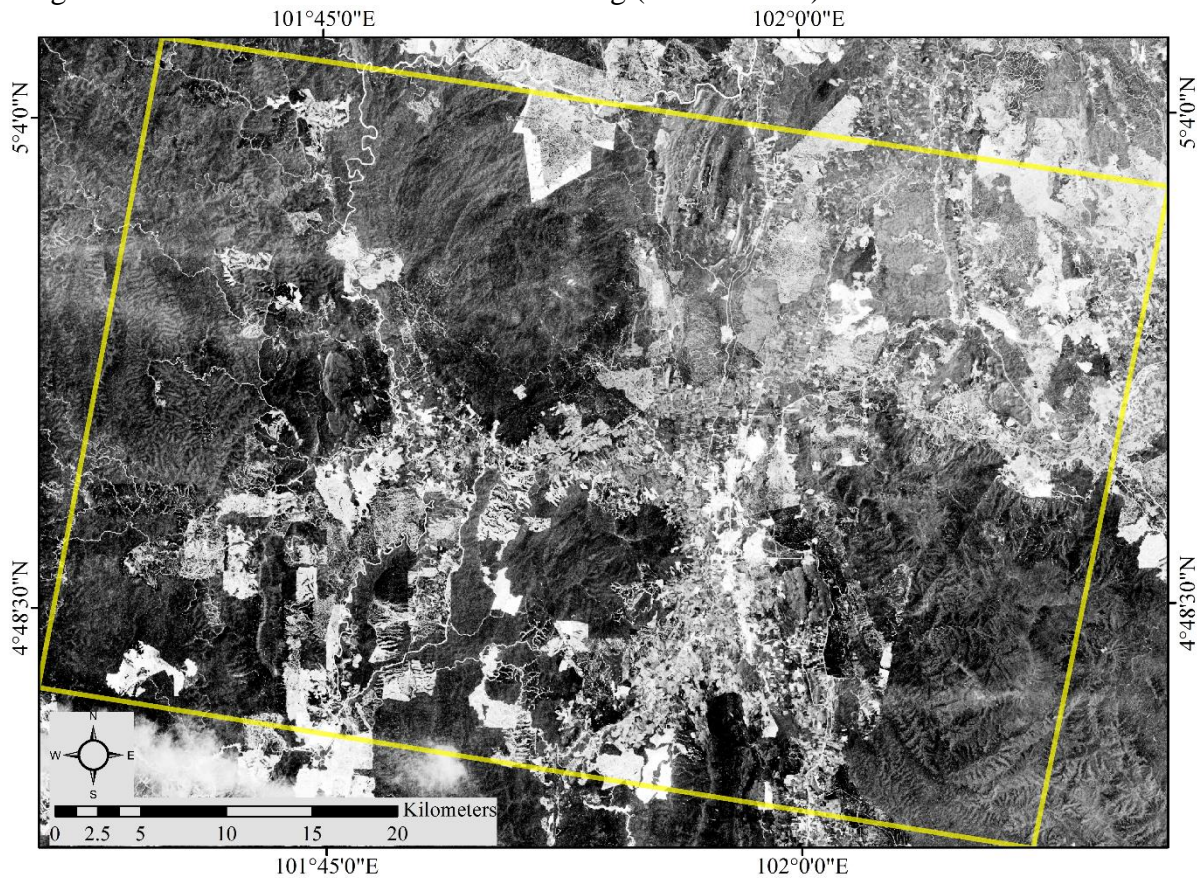


Fig. 3: Grayscale image of DPC 1 - the image shows the lithology beneath the vegetated but only altered rocks of the hydroxyl-bearing are prominently revealed.

For DPC2 (Fig 4), the presence of vegetation spectra is very low (-0.738147) while spectra from Clay minerals, Ferric Oxide, and Ferrous Oxide have strong positive

contributions (i.e. 0.079281, 0.647945 and 0.170355). The amount of clay mineral spectral in DPC2 shows the degree to which vegetation spectral is suppressed (Pour et. al, 2014). This consequently highlights the background rocks that elicit the physical characteristics of the lithology. The lithology reveals the characteristic slope, relief and resistance to weathering (Paul et al., 2006) which is reflected in the morphology. Based on the physical properties, the rock appears largely fractured containing large amount of altered minerals in halos, a secondary dispersion pattern due to the supergene migration of elements in the regolith or soil, often superjacent over a 'blind' ore deposit in the bedrock (Paul et al., 2006). The topography shows abrupt change in channels that controls water flow through fractures with interchanging lineament, ridges, and channels. In addition to exposing the background lithology, DPC2 contributes significantly to revealing the iron oxide and clay-rich rich soils when they are used as composite image display (Fraser and Green (1987).

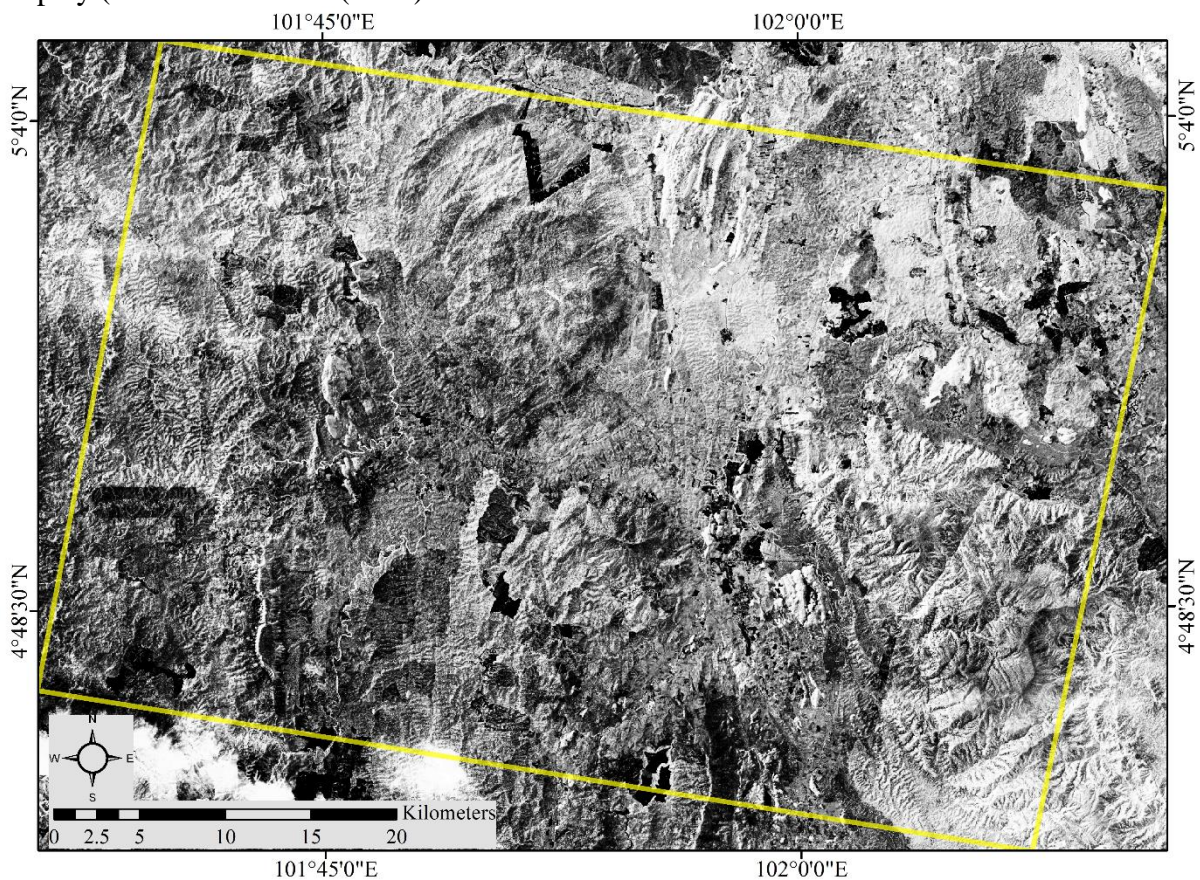


Fig. 4: Grayscale image of DPC 2 - Complete topographic configuration of the lithology beneath vegetation is emphasized in the image.

DPC3 (Fig 5) has positive presence of vegetation spectra. However, the strong contribution of Ferric and Ferrous iron oxide (0.984370 and 0.012551) makes it useful for mapping the two oxide-rich rocks even though the quantity of Clay mineral spectral is low. For example, combination of DPC 1 and DPC 2 will counter the deficiency in

DPC 3. Like DPC 1, DPC3 de-emphasize lithological characteristics but it does not clearly distinguish any particular property as DPC1.

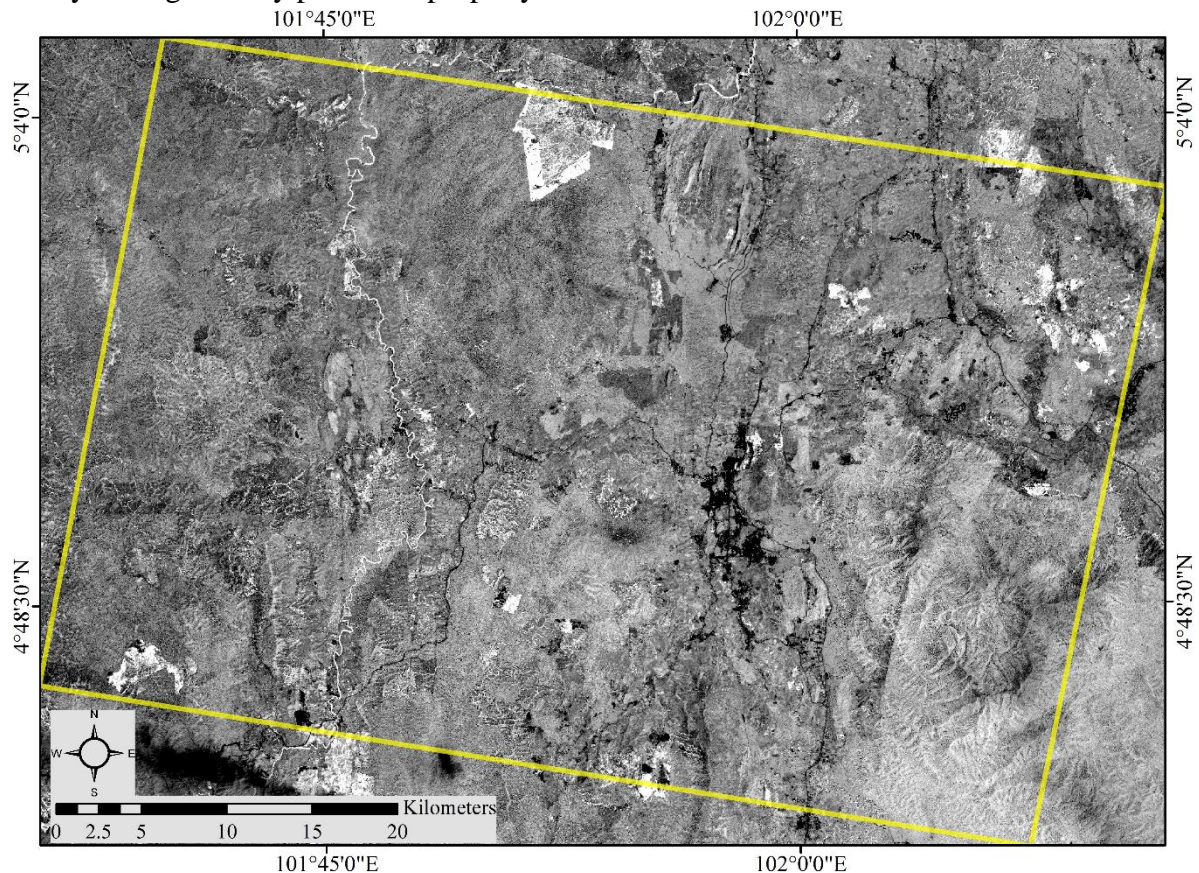


Fig. 5: Grayscale image of DPC 3 – Poor in revealing the lithology but rich in geochemical information content.

The greyscale display of the DPC images does not provide discernible variation between different rocks. False colour composite provides unique pattern of spatial arrangement and contiguity. Fig. 6 presents the lithology in a more intuitive visualization using the colour variations (brown-yellowish and purple spread) (Crosta and Rabelo, 1993; Ali and Pour, 2014). It can be seen that the surficial bedrock varies in colour that indicate difference in properties. But low spatial resolution of the image prevents a more discrete delineation of individual rock unit area.

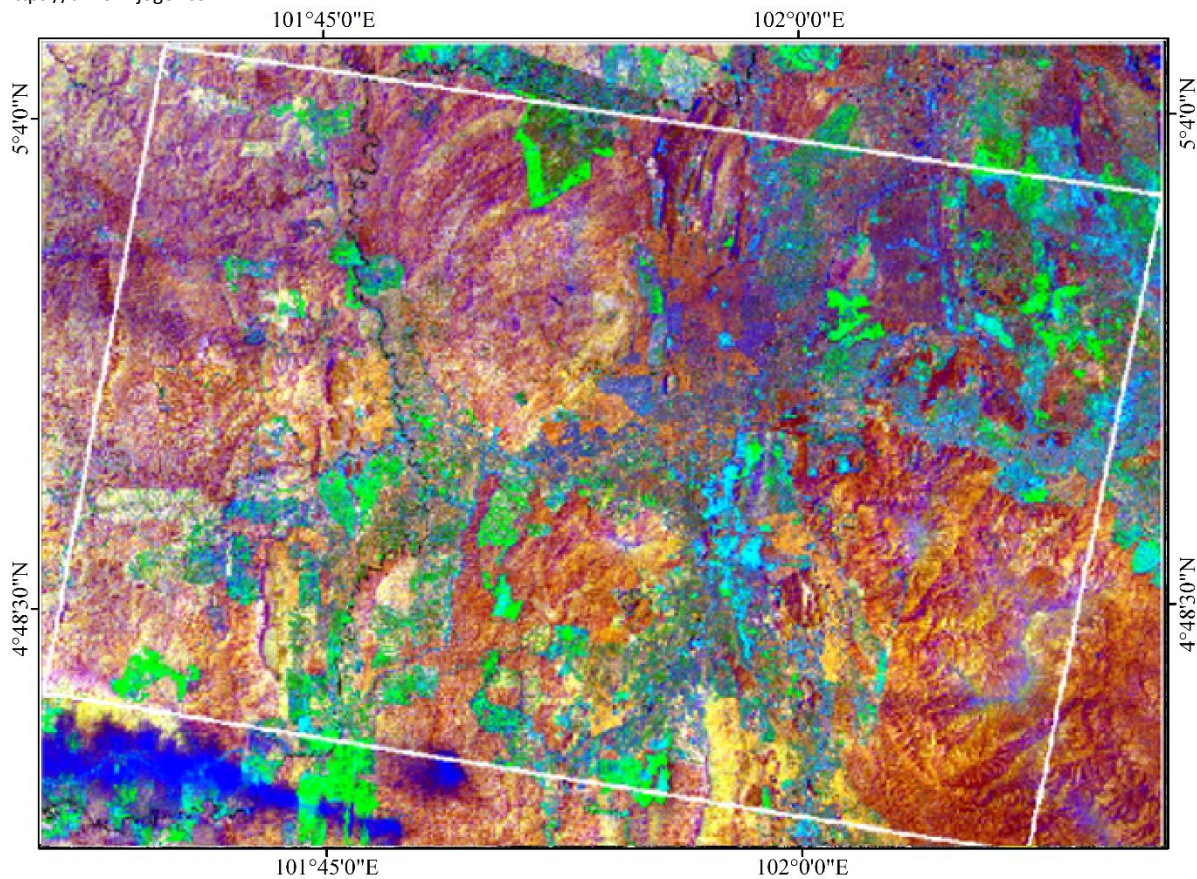


Fig. 6: RGB colour inverted DPC 1, DPC 2, and DPC 3 images. Colour inversion process highlights different lithological units by emphasizing variation in toner gradient.

By super imposing the lithological map (Fig. 7a) of the study area on the composite image (Fig. 7b), relationship between colour variation indicating different rock unit and their boundary can be established. The Limestone rock located in the south-eastern part is shown in predominantly golden brown colour with a spread of purple colour that dominates the Triassic sedimentary rock in the north-east (Fig. 7). The older rocks, Igneous and Permian sedimentary, which trends north-south at the central zone appear brown in the composite image. Also in the eastern side is the metamorphic rock which share visual colour appearance of the igneous and Permian sedimentary rocks (mixture of brown and purple). The northern side comprises of younger formed from deposition of weathered rocks from the older rocks (see the lithology in Fig. 4). This reflects the potentials of Landsat 8 for lithological mapping at regional scale in spite of the limitation imposed by radiometric resolution which prevents micro-scale spectral analysis (Mahmood and Easson, 2006).

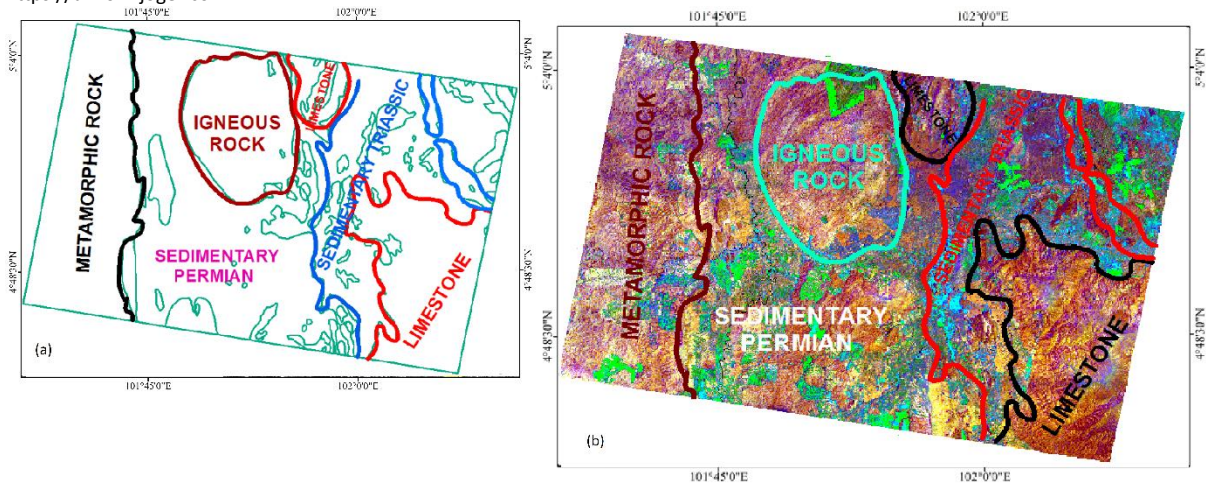


Fig. 7: (a) Lithological map of the study area and (b) super-imposed lithological map on the RGB colour inversion that shows the lithology in colour variation.

4.2 Mapping clay and oxide-based minerals

Fraser and Green (1987) proposed a standard colour composite of DPC images for extracting clay and oxide-based minerals. According to Wilford and Creasey (2002), RGB false colour combination of DPC 1, DPC 2, and DPC 3 will yield distinct colours (i.e. Clay mineral rock in red, Iron Oxide in green and Silica in blue). Fig. 8 is the result of this combination. Limestone, igneous and Permian sedimentary rocks are richer in silica while sedimentary Triassic is rich in Iron oxide and clay minerals. Like the younger sedimentary rock, the Permian sedimentary rock also contains large content of clay minerals with little iron oxide intrusion. For the metamorphic rock has a balances presence of Silica and Iron oxide and isolated clay minerals towards the boundary with Permian sedimentary rock. The large content of silica across the rocks, especially within the older rocks explains the diagenetic transformation during lithification. Absence of clay minerals in the within the igneous rock is an indication of its volcanic origin where the oxide-based chemical properties accounts for solidification of the extruded lava.

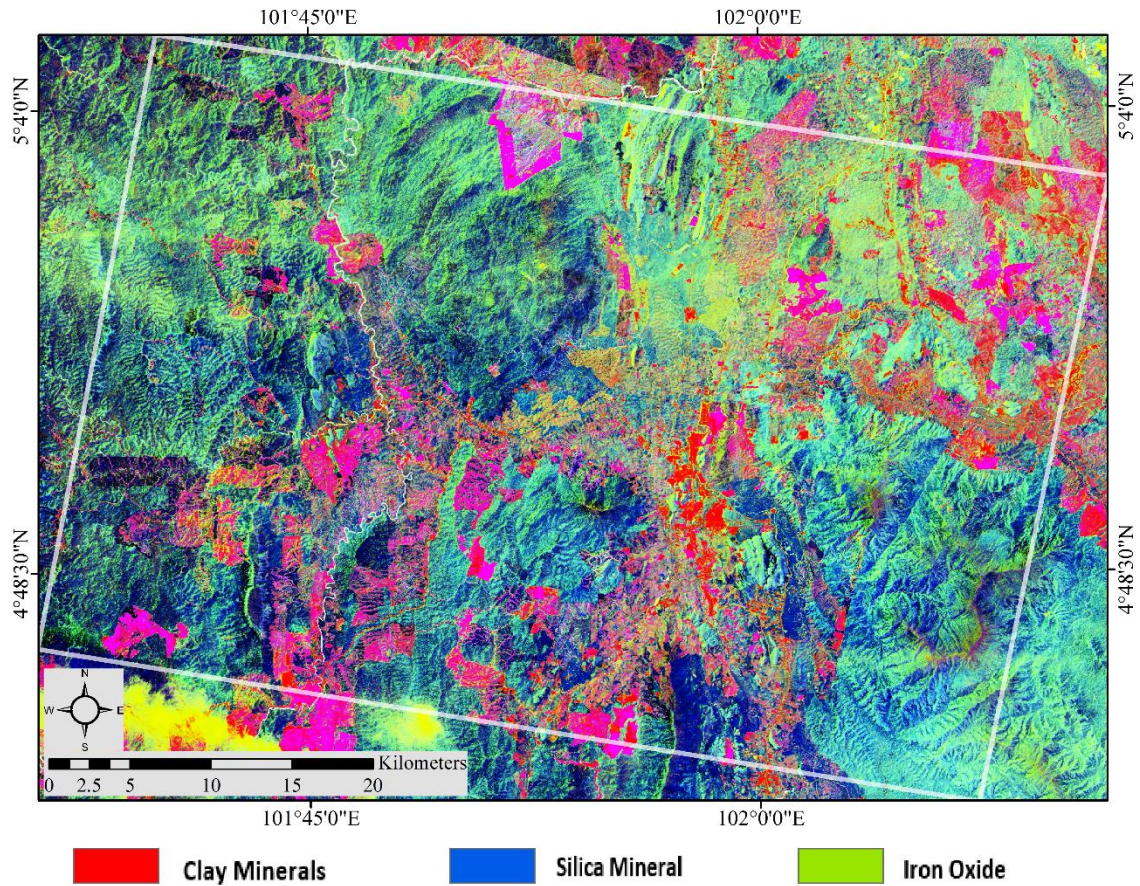


Fig. 8: Clay and oxide-based mineral map based on Fraser and Green (1987) DPC image false colour combinations - Clay mineral in red, Iron oxide in green, and Silica in blue.

5. Conclusion

This study explores the potential of Landsat 8 for detecting and mapping surface geologic formation in Gua Musang Gold field. The investigation demonstrates the prospect of Landsat 8 for regional scale lithological mapping in tropical environment using spectral transformation (DPCA) technique. DPCA effectively suppressed vegetation spectral to highlight, not only the lithology surface, but the rock mineral composition. Both the greyscale images and their colour composite are useful for geological studies in vegetated environment, not only for the physical properties of the rock, but also the geochemical properties. The limitation of the method is its inability to provide discrete boundaries of the respective outcrop; however, development of other indices in addition to those used in this study could further enhance the capability of Landsat 8 data for geological study.



Acknowledgement

Landsat 8 imagery was downloaded from Earth Resource Observation and Science Centre of the US Geological Survey (USGS) and the lithological map was provided by the Department of Minerals and Geoscience Malaysia (JMG).

References

- Aboelkhair, H., Ninomiya, Y., Watanabe, Y., & Sato, I. (2010). Processing and interpretation of ASTER TIR data for mapping of rare-metal-enriched Albite Granitoids in the central eastern desert of Egypt. *Journal of African Earth Sciences*, 58(1), 141-151 doi.org/10.1016/j.jafrearsci.2010.01.007
- Ali, A. S., & Pour, A. B. (2014). Lithological mapping and hydrothermal alteration using Landsat 8 data: a case study in ariab mining district, red sea hills, Sudan. *International Journal of Basic and Applied Sciences*, 3(3), 199-203.
- Amer, R., Kusky, T., & Ghulam, A. (2010). Lithological mapping in the central eastern desert of Egypt using ASTER data. *Journal of African Earth Sciences*, 56(2), 75-82. doi.org/10.1016/j.jafrearsci.2009.06.004
- Bahiru, E. A. (2011). Inter-relationship between lithology and structure and its control on gold mineralization in Buhweju area, sw of Uganda.
- Crippen, R. E., & Blom, R. G. (2001). Unveiling the lithology of vegetated terrains in remotely sensed imagery. *Photogrammetric engineering and remote sensing*, 67(8), 935-946.
- Crosta, A. P., & Rabelo, A. (1993). Assessing Landsat/TM for hydrothermal alteration mapping in Central-Western Brazil. In *Proceedings of the Thematic Conference on Geologic Remote Sensing (Vol. 1, pp. 1053-1053)*. Environmental Research Institute of Michigan.
- Crosta, A., & Moore, J. (1989). Enhancement of Landsat Thematic Mapper imagery for residual soil mapping in SW Minas Gerais State, Brazil- A prospecting case history in greenstone belt terrain. In *Thematic Conference on Remote Sensing for Exploration Geology- Methods, Integration, Solutions, 7 th, Calgary, Canada (pp. 1173-1187)*.
- Department of Minerals and Geoscience Malaysia (2003). *Quarry Resource Planning for the State of Kelantan*. Osborne & Chappel Sdn. Bhd.
- Elvidge, C.D., and R.J.P. Lyon, (1985). Estimation of the vegetation contribution to the 1.65/1.22 μm ratio in airborne thematic-mapper imagery of the Virginia Range, Nevada, *International Journal of Remote Sensing*, 6(1):75-88.
- Fraser, S., & Green, A. (1987). A software defoliant for geological analysis of band ratios. *International Journal of Remote Sensing*, 8(3), 525-532. doi.org/10.1080/01431168708948659
- Gad, S., & Kusky, T. (2007). ASTER spectral ratioing for lithological mapping in the Arabian–Nubian shield, the Neoproterozoic Wadi kid area, Sinai, Egypt. *Gondwana Research*, 11(3), 326-335. doi.org/10.1016/j.gr.2006.02.010
- Galvão, L. S., Almeida-Filho, R., & Vitorello, I. (2005). Spectral discrimination of hydrothermally altered materials using ASTER short-wave infrared bands:



- Evaluation in a tropical savannah environment. *International Journal of Applied Earth Observation and Geoinformation*, 7(2), 107-114. doi.org/10.1016/j.jag.2004.12.003
- Ghani, A.A. (2009). Plutonism. In: Hutchison, C.S. and Tan, D.N.K., Eds., *Geology of Peninsular Malaysia*, Geological Society of Malaysia, Kuala Lumpur, 211-232.
- Guide, E. U. S. (2009). Atmospheric correction module: QUAC and FLAASH user's guide. Version, 4, 1-44.
- Gwendolyn W. Luttrell (1952), *Bibliography of U. S. Geological Survey Publications on Copper (To January 1,1952)*, Geological Survey Circular 178, United States Department of the Interior, Washington, D. C-, 1952.
- Heng, G. S., Hoe, T. G., & Hassan, W. F. W. (2006). Gold Mineralization and Zonation In The State Of Kelantan. *Geological Society of Malaysia Bulletin*, 52(June), 129–J35.
- Horwitz, H. M., Nalepka, R. F., Hyde, P. D., & Morgenstern, J. P. (1971). Estimating the proportions of objects within a single resolution element of a multispectral scanner (object proportions estimation algorithms in single resolution element of airborne multispectral scanner). *International Symposium on Remote Sensing of Environment*, 7 Th, University of Michigan, Ann Arbor, Mich, 1307-1320.
- Howard, A. D. (1967). Drainage analysis in geologic interpretation: a summation. *AAPG bulletin*, 51(11), 2246-2259.
- Inzana, J., Kusky, T., Higgs, G., & Tucker, R. (2003). Supervised classifications of Landsat TM band ratio images and Landsat TM band ratio image with radar for geological interpretations of central Madagascar. *Journal of African Earth Sciences*, 37(1), 59-72. doi.org/10.1016/S0899-5362(03)00071-X.
- Khamar Shah, a. (2012). Mesothermal lode gold deposit Central Belt Peninsular Malaysia. Imran Ahmad, D. (Ed.). *Earth Sciences*, 314–342. Retrieved from <http://www.scribd.com/doc/151432098/InTech-Mesothermal-Lode-Gold-Deposit-Central-Belt-Peninsular-Malaysia>.
- Mahmood, T., & Easson, G. (2006, May). Comparing ASTER and Landsat 7 ETM+ for Change Detection. In *Proceedings of ASPRS Annual Conference*, May 1–5, 2006, Reno, Nevada.
- Markham, B., Barsi, J., Kvaran, G., Ong, L., Kaita, E., Biggar, S. & Helder, D. (2014). Landsat-8 operational land imager radiometric calibration and stability. *Remote Sensing*, 6(12), 12275-12308. doi:10.3390/rs61212275
- Marsili, R. (2006). *Sensory-directed flavour analysis* CRC Press.
- Murphy, R. J., & Wadge, G. (1994). The effects of vegetation on the ability to map soils using imaging spectrometer data. *Remote sensing*, 15(1), 63-86. doi.org/10.1080/01431169408954051
- Mustard, J. F. (1993). Relationships of soil, grass, and bedrock over the Kaweah serpentinite melange through spectral mixture analysis of AVIRIS data. *Remote Sensing of Environment*, 44(2), 293-308. doi:10.1016/0034-4257(93)90023-Q
- Nazaruddin, D. A., Fadilah, N. S. M., Zulkarnain, Z., Omar, S. A. S., & Ibrahim, M. K. M. (2014). *Geological Studies to Support the Tourism Site: A Case Study in the*



- Rafflesia Trail, Near Kampung Jedip, Lojing Highlands, Kelantan, Malaysia. *International Journal of Geosciences*, 5(08), 835. DOI: 10.4236/ijg.2014.58074
- Neville, R., Levesque, J., Staenz, K., Nadeau, C., Hauff, P., & Borstad, G. (2003). Spectral unmixing of hyperspectral imagery for mineral exploration: Comparison of results from SFSI and AVIRIS. *Canadian Journal of Remote Sensing*, 29(1), 99-110. doi.org/10.5589/m02-085
- Oliver, G., Zaw, K., Hotson, M., Meffre, S., & Manka, T. (2014). U–Pb zircon geochronology of Early Permian to Late Triassic rocks from Singapore and Johor: A plate tectonic reinterpretation. *Gondwana Research*, 26(1), 132–143. doi.org/10.1016/j.gr.2013.03.019
- Paul, H.J., Gillis, K.M., Coggon, R.M., and Teagle, D.A.H., (2006). ODP Site 1224: a missing link in the investigation of seafloor weathering. *Geochem., Geophys., Geosyst.*, 7(2). doi:10.1029/2005GC001089
- Plaza, A., Martínez, P., Pérez, R., & Plaza, J. (2004). A quantitative and comparative analysis of endmember extraction algorithms from hyperspectral data. *Geoscience and Remote Sensing, IEEE Transactions on*, 42(3), 650-663. DOI: 10.1109/TGRS.2003.820314
- Pour, A. B., & Hashim, M. (2013). Fusing ASTER, ALI and hyperion data for enhanced mineral mapping. *International Journal of Image and Data Fusion*, 4(2), 126-145. <http://dx.doi.org/10.1080/19479832.2012.753115>
- Pour, A. B., & Hashim, M. (2014). Structural geology mapping using PALSAR data in the Bau gold mining district, Sarawak, Malaysia. *Advances in Space Research*, 54(4), 644-654. <http://dx.doi.org/10.1016/j.asr.2014.02.012>
- Pour, A. B., Hashim, M., & Marghany, M. (2014). Exploration of gold mineralization in a tropical region using Earth Observing-1 (EO1) and JERS-1 SAR data: a case study from Bau gold field, Sarawak, Malaysia. *Arabian Journal of Geosciences*, 7(6), 2393-2406 <http://dx.doi:10.1007/s12517-013-0969-3>
- Pour, A. B., & Hashim, M. (2011). Identification of hydrothermal alteration minerals for exploring of porphyry copper deposit using ASTER data, SE Iran. *Journal of Asian Earth Sciences*, 42(6), 1309-1323. <http://dx.doi.org/10.1016/j.jseaes.2011.07.017>
- Pour, A. B., & Hashim, M. (2011a). Spectral transformation of ASTER data and the discrimination of hydrothermal alteration minerals in a semi-arid region, SE Iran. *International Journal of the Physical Sciences*, 6(8), 2037-2059.
- Pour, B., & Hashim, M. (2011b). The earth observing-1 (EO-1) satellite data for geological mapping, southeastern segment of the central Iranian volcanic belt, Iran. *Int.J.Phys.Sci*, 6(33), 7638-7650. <http://dx.doi: 10.5897/IJPS11.910>
- Pour, A. B., & Hashim, M. (2012a). The application of ASTER remote sensing data to porphyry copper and epithermal gold deposits. *Ore Geology Reviews*, 44, 1-9. <http://dx.doi.org/10.1016/j.oregeorev.2011.09.009>
- Pour, A. B., & Hashim, M. (2012b). Identifying areas of high economic-potential copper mineralization using ASTER data in the Urumieh–Dokhtar volcanic belt, Iran. *Advances in Space Research*, 49(4), 753-769. <http://dx.doi.org/10.1016/j.asr.2011.11.028>



- Pour, A. B., & Hashim, M. (2013). Fusing ASTER, ALI and hyperion data for enhanced mineral mapping. *International Journal of Image and Data Fusion*, 4(2), 126-145. <http://dx.doi.org/10.1080/19479832.2012.753115>
- Pour, B., & Hashim, M. Van genderen. J. 2013a detection of hydrothermal alteration zones in a tropical region using satellite remote sensing data: Bau gold field, Sarawak, Malaysia. *Ore Geology Reviews*, 54, 181-196. <http://dx.doi.org/10.1016/j.oregeorev.2013.03.010>
- Pournamdari, M., & Hashim, M. (2014). Detection of chromite bearing mineralized zones in Abdasht ophiolite complex using ASTER and ETM+ remote sensing data. *Arabian Journal of Geosciences*, 7(5), 1973-1983. doi:10.1007/s12517-013-0927-0
- Qari, M., Madani, A., Matsah, M., & Hamimi, Z. (2008). Utilization of aster and landsat data in geologic mapping of basement rocks of Arafat area, Saudi Arabia. *Arabian Journal for Science and Engineering*, 33(1C), 100.
- Rahman, C. A., & Mohamed, K. R. (2001). Pemetaan Awal Sumber Warisan Geologi Negeri Kelantan. *Geological Heritage of Malaysia (Geoheritage Mapping and Geosite Characterization)*, LESTARI UMK, Bangi, 27-39.
- Ramadan, T. M., & Fattah, M. F. A. (2010). Characterization of gold mineralization in Garin Hawal area, Kebbi State, NW Nigeria, using remote sensing. *The Egyptian Journal of Remote Sensing and Space Science*, 13(2), 153-163. doi.org/10.1016/j.ejrs.2009.08.001
- Rowan, L. C., Hook, S. J., Abrams, M. J., & Mars, J. C. (2003). Mapping hydrothermally altered rocks at cuprite, Nevada, using the advanced spaceborne thermal emission and reflection radiometer (ASTER), a new satellite-imaging system. *Economic Geology*, 98(5), 1019-1027. doi: 10.2113/gsecongeo.98.5.1019
- Rowan, L. C., Mars, J. C., & Simpson, C. J. (2005). Lithologic mapping of the Mordor, NT, Australia ultramafic complex by using the advanced spaceborne thermal emission and reflection radiometer (ASTER). *Remote Sensing of Environment*, 99(1), 105-126. doi.org/10.1016/j.rse.2004.11.021
- Rowan, L. C., Pawlewicz, M. J., & Jones, O. D. (1992). Mapping thermal maturity in the chainman shale, near eureka, Nevada, with Landsat thematic mapper images (1). *AAPG Bulletin*, 76(7), 1008-1023
- Ryerson, R. A., & Rencz, A. N. (1999). *Manual of remote sensing, remote sensing for the earth sciences* John Wiley & Sons.
- Siegal, B. S., & Goetz, A. F. (1977). Effect of vegetation on rock and soil type discrimination.
- Singh, A., & Harrison, A. (1985). Standardized principal components. *International Journal of Remote Sensing*, 6(6), 883-896. doi.org/10.1080/01431168508948511
- Smith, M.O., J.B. Adams, and D.A. Roberts (1988). Removing the spectral effects of vegetation in multispectral images. *Proceedings of the Sixth Thematic Conference on Remote Sensing for Explomtion Geology*, 16-19 May, Houston, Texas, 1:183
- Sultan, M., Arvidson, R. E., & Sturchio, N. C. (1986). Mapping of serpentinites in the Eastern Desert of Egypt by using Landsat thematic mapper data. *Geology*, 14(12), 995-999.



- Swayze, G. A., & Clark, R. N. (1995). Spectral identification of minerals using imaging spectrometry data: Evaluating the effects of signal to noise and spectral resolution using the tricorder algorithm. *Summaries of the 5th Annual JPL Airborne Earth Science Workshop*, 95-91.
- Tjia, H.D. (1973). Geomorphology. In: De Sitter, LU, Ed., *Geology of the Malay Peninsula*, John Wiley & Sons, Inc., Hoboken, 13-24
- Unjah, T., Komoo, I., & Mohamad, H. (2001). Pengenalpastian sumber warisan geologi di negeri Kelantan. *Geological Heritage of Malaysia (Geoheritage Mapping and Geosite Characterization)*, LESTARI UMK, Bangi, 111-126.
- Van der Meer, F. (1995). Spectral reflectance of carbonate mineral mixtures and bidirectional reflectance theory: Quantitative analysis techniques for application in remote sensing. *Remote Sensing Reviews*, 13(1-2), 67-94
doi.org/10.1080/02757259509532297
- Van der Meer, F., & De Jong, S. M. (2000). Improving the results of spectral unmixing of Landsat Thematic Mapper imagery by enhancing the orthogonality of end-members. *International Journal of Remote Sensing*, 21(15), 2781-2797.
doi.org/10.1080/01431160050121249
- Wilford, J., & Creasey, J. (2002). Landsat thematic mapper. *Geophysical and remote sensing methods for regolith exploration*. (Ed. E Papp) pp, 6-12.
- Yu, L., Porwal, A., Holden, E. J., & Dentith, M. C. (2011). Suppression of vegetation in multispectral remote sensing images. *International journal of remote sensing*, 32(22), 7343-7357. doi.org/10.1080/01431161.2010.523726